Influence of high-pressure on the short-range structure of Ca or Na aluminoborosilicate glasses from 11B and 27Al solid-state NMR

Sami Soudani, Michael Paris, Yann Morizet

Influence of high-pressure on the short-range structure of Ca or Na aluminoborosilicate glasses from ^{11}B and ^{27}Al solid-state NMR

Sami SOUDANI[1,2*], Michael PARIS[2], Yann MORIZET[1,2],

[1] Nantes Université, CNRS, UMR 6112, Laboratoire de Planétologie et Géosciences, F-44000 Nantes, France

[2] Nantes Université, CNRS, Institut des Matériaux de Nantes Jean Rouxel, IMN, F-44000 Nantes, France

*Corresponding author: Sami Soudani

Postal address:

Laboratoire de Planétologie et Géosciences (LPG), UMR-CNRS 6112, Nantes Université.

2 rue de la Houssinière, 44322 Nantes Cedex (FRANCE)

phone: +33 (0) 2 5112 5491

fax: +33 (0) 2 5112 5268

*E-mail: sami.soudani@univ-nantes.fr

Abstract

The present study investigates the boron and aluminium speciation of aluminoborosilicate glasses synthesized under ambient to high-pressure conditions (up to 2.0 GPa) using ^{11}B and ^{27}Al Nuclear Magnetic Resonance. Four glass series were prepared in the SiO_2-Al_2O_3-B_2O_3-Na_2O/CaO system, with either high or low R' values (R'=([Na_2O]+[CaO])/([B_2O_3]+[Al_2O_3])). ^{11}B NMR reveals a linear increase in four-coordinated boron (BO_4) with pressure for Ca glasses and non-linear with a plateau between 0.5 and 1.5 GPa for Na glasses. ^{27}Al NMR reveals minimal pressure impact on aluminium coordination in sodium glasses. Conversely, calcium glasses form higher-coordinated AlO_5 and AlO_6 units under pressure. The determination of non-bridging oxygen (NBO) variation witnesses the change in compensation mechanism for boron species. In low R' glasses, limited NBOs suggest Na^+/Ca^{2+} release from AlO_4 as the primary compensation source. This work sheds light on pressure's influence on network connectivity in simple glasses, aiding the understanding of complex glass behaviour.

1 Introduction

Glass is a universal material that can be prepared and tailored to optimise its mechanical, optical or electrical properties. In particular, alkali and/or alkaline-earth aluminoborosilicate glasses are used in a wide range of technologies and are especially designed for the immobilization of radioactive wastes [1-5]. The knowledge of the glass structure is a prerequisite for determining how the radioisotopes are incorporated into the aluminoborosilicate glasses. In addition, how the radioisotope incorporates into the glass structure is of prime interest in order to discuss the glass chemical durability.

The structure of aluminoborosilicate glasses made under ambient pressure conditions has been widely investigated and is now fairly understood [6-15]. Boron and aluminium are typically

found in these glasses as BO_3 planar triangle and BO_4 tetrahedron units, and AlO_4 tetrahedron, as well as AlO_5 and AlO_6 polyhedron. The tetrahedral coordination of these +3 charged elements carries an excess negative charge, which is compensated by alkali or alkaline-earth cations in the immediate surrounding [6,16-18]. The AlO_4 and BO_4 units act as regular network formers, connecting tetrahedra in a homogeneous 3D system. The BO_3 units also act as network formers, however the planar triangle shape tends to create less connected regions in the glass structure at the nanometer scale in BO_3-rich regions. On the other hand, highly coordinated Al species have a more intricate role in glasses. Their presence originates from local charge-balance considerations, and their precise structural role still remain unclear (see ref. [19] for an extensive review on ^{27}Al NMR and focus on the role and environment of each aluminium species). AlO_5 and AlO_6 are out of usual "network forming" group as they do not participates into the backbone network in the usual way [20-21] and are also out of the "network modifying" group as they present higher field strength and stronger bonding to their oxygen than usual modifiers. Moreover, known modifier cations (i.e. alkali and earth-alkali cations) are coordinating principally NBO [22-25] where AlO_5 and AlO_6 are mainly linked to bonding oxygens [23,25-26].

The distributions of the AlO_4 and BO_4 units have a significant impact on the macroscopic properties of the glass, as it is closely related to the glass polymerisation. A glass with a low polymerisation is characterised by a low bridging oxygen content (or high non-bridging oxygen, NBO). For example, it is commonly observed that density and viscosity decrease with boron addition to aluminosilicate glass network [27-31]. Those properties depend on the BO_4 to BO_3 species distribution that is commonly expressed with the N_4 value ($N_4 = [BO_4]/([BO_4]+[BO_3])$) [8,16-18]. The N_4 value does not correlate linearly with the glass composition, which results in a non-linear evolution of the macroscopic properties for aluminoborosilicate glasses. Such behaviour is known as the "boron anomaly" [6-7,16-18]. Several studies have investigated this

70 "boron anomaly" by elucidating the relationship between the network former content, the
71 network modifier content and the macroscopic properties through the N_4 value determination.
72 Early work by Dell and co-authors [17] and subsequently updated work by Du and Stebbins [8]
73 established a direct link between the N_4 value and the chemical composition using the R' and
74 K' (K'=[SiO_2]/([B_2O_3]+[Al_2O_3])) parameters determined from the glass chemical composition.
75 Previous investigation [16] demonstrated that there is a complex evolution of the N_4 as a
76 function of R' and K' determined by alkali and alkaline-earth cation roles within the glass
77 structure.

78 There is a growing interest in using high-pressure syntheses for producing novel materials and
79 especially glasses [29-36]. Recent works demonstrated that the use of high-pressure conditions
80 during the aluminoborosilicate glass-making process successfully improves the solubility of Cl
81 and I; therefore representing a potential industrial solution for the immobilisation of those
82 halogen radioisotopes [37-341]. However, there is a lack of information on the effect that
83 pressure induces on these complex glass structures. The Earth science community has long
84 known the effect of pressure on the structure of aluminosilicate glass compositions [42-49];
85 however, only a few studies addressed the effect of pressure on aluminoborosilicate glasses
86 [32-36,50-51]. High-pressure conditions are known to induce major structural modifications
87 impacting the glass macroscopic properties such as viscosity or density that are proxies to the
88 glass durability. In order to propose a reliable protocol for the volatile nuclear waste
89 immobilisation in high-pressure glass matrix, complementary information is required about the
90 aluminoborosilicate structural modifications under such extreme conditions. With increasing
91 pressure, the percentage of BO_4 units increases [34-35,47,52-56]. This mechanism corresponds
92 to an increase in the network connectivity considering that BO_4 unit represents the most
93 polymerized boron species. Such an increase in the network connectivity is an important issue

as it is a key parameter for glass durability and is therefore crucial for nuclear waste immobilisation.

Recently, Bista and co-authors [35] studied the effect of compression (up to 3.0 GPa) on Al, B and Si, with glass compositions in the $15CaO\text{-}15Al_2O_3\text{-}xB_2O_3\text{-}(70\text{-}x)SiO_2$ system (i.e. relatively high-Al content). With increasing pressure, they observed a rapid increase in the proportion of highly coordinated Al species, resulting in an increase in the average Al coordination. Furthermore, they showed that Al coordination increases faster for glass compositions with higher B_2O_3 and lower SiO_2 content. They suggested that the stability of AlO_4 species over pressure is lowered with increasing BO_4 species, and that less Si-O-Al linkages are possible. Indeed, as B_2O_3 increases, the N_4 value increases causing a higher charge compensation requirement for BO_4 species. Lee and co-authors [36] also observed the same behaviour for glass compositions in the system $0.5Na_2O\text{-}0.25Al_2O_3\text{-}0.25B_2O_3\text{-}xSiO_2$ (12.5 mol.% Al_2O_3 for x = 1, and 6.3 mol.% Al_2O_3 for x = 3) with application to the isotopic fractionation of boron within the Earth interior (up to pressure of 9.2 GPa). In a similar manner, Wondraczek [32], Smedskjaer [33] and their co-authors investigated the change in the N_4 value in Al-free glasses synthesised at pressure up to 0.6 GPa and also determined an increase in the N_4 value with increasing pressure.

Although these studies constitute landmark works, there is still a lack of experimental data for determining the changes in the glass structure in the pressure range up to 2.0 GPa that is most relevant for nuclear waste immobilisation [57] and for a wider range of glass compositions. Furthermore, there is a lack of detailed investigations about the change in boron speciation. Actually, most of the previous studies only focused on the N_4 value variation with pressure and no thorough information is available on the actual changes in speciation (i.e. type of BO_3 units converting into BO_4 units, and their relation to the NBO content). For instance, the sole distribution between BO_3 and BO_4 units is a simplified view of the boron speciation and that

each boron species is composed of several individual sub-unit with different geometrical configuration or various next nearest neighbours [52,58-60]. Whether each of them evolves linearly with pressure remains to be determined.

In the present work, we investigate the aluminoborosilicate glass structural changes synthesised between ambient and 2.0 GPa pressure and at high-temperature (1250°C). The studied compositions are either Ca- or Na-bearing aluminoborosilicate glasses. We use Solid-State Nuclear Magnetic Resonance (NMR) to investigate the ^{11}B, and ^{27}Al local environments in the synthesised samples. We attempt to discuss our result in term of glass physical properties for nuclear waste immobilisation and volatile dissolution capability.

2 Material and methods

2.1 Ambient-pressure glass

Several aluminoborosilicate glass compositions were studied under different pressure conditions up to 2.0 GPa. Two series of glasses were synthetized in the systems Al_2O_3-SiO_2-B_2O_3-Na_2O/CaO: pure calcic with two different B_2O_3 (18 and 11 mol.%) and CaO (21 and 33 mol.%) contents (Ca21B18 and Ca33B11), and pure sodic with two different B_2O_3 (23 and 7.5 mol.%) and Na_2O (22 and 35 mol.%) contents (Na22B23 and Na35B8). Those glass compositions are identical to the one investigated in Morizet et al. [61] in which they studied the iodine dissolution mechanisms as a function of the optical basicity. The K' and R' ratios defined as a representative compositional parameter for borosilicate and aluminoborosilicate glasses [8,17,62] for our samples vary from 1.7 to 3.9 and from 0.7 to 2.7, respectively (see Table 1).

Each ambient-pressure glass was prepared from spec pure oxides (CaO, B_2O_3, SiO_2 and Al_2O_3) and carbonates (Na_2CO_3) that were carefully ground in an agate mortar. Sample powder was melted in a Pt crucible at 1200°C in a box furnace for 1h. The ambient pressure sample quench was done by dropping the Pt crucible in water (~150°C/s for the quench rate). We checked

optically the recovered glasses for the presence of crystalline phase. The ambient pressure glasses have been analysed for chemical composition as reported in Table 1.

2.2 High-pressure experimental syntheses

The high-pressure experiments were conducted using an end-loaded piston-cylinder apparatus at the Laboratoire de Planétologie et Géosciences Nantes (LPG). Parent glass (ambient-pressure glass) powders were loaded into 2.9 mm outer diameter and 10 mm long Pt capsules. The Pt capsules were welded shut at both ends by arc-welding. During each experiment, two capsules are collated together into the ¾ inch talc-Pyrex high-pressure assembly. In the present study, we investigated several pressure conditions: 1 atm., 0.5, 1.0, 1.5 and 2.0 GPa. For clarity in the manuscript, we have adopted the following nomenclature for samples: the name of the composition followed by the pressure synthesis value. For instance, the sample Ca21B18-0 and Na35B8-1.5 stand for Ca21B18 and Na35B8 glasses synthesised at 0.0001 and 1.5 GPa, respectively.

The protocol for reaching the experimental conditions is described in previous works [38-39]. The talc-Pyrex assembly is first pressurized to 1.0 GPa and temperature is increased to 550°C and is kept constant for 10 minutes in order to stabilise the temperature and to relax the high-pressure assembly. Pressure is then increased to the final pressure if needed, and temperature is raised to 1250°C. For 0.5 GPa conditions, the temperature increase is accompanied by a decrease in pressure, and the 0.5 GPa final pressure is reached once the final temperature is attained (1250°C). During the experiment, the pressure is automatically controlled by a Stigma© needle pump, preventing from pressure variation and the temperature is monitored by a Eurotherm© controller with a B-type ($PtRh_6$-$PtRh_{30}$) thermocouple wire located at the top of the capsules. Pressure and temperature are accurate within 10% in relative to the value and 1°C, respectively. The run duration was set to 2h for all the experiments to be reproducible. We

169 performed an isobaric quench at the end of the experiment by cutting-off the power. The cooling
170 rate is estimated at ~100°C in the first 500°C. The isobaric quench has the advantage to prevent
171 from a lower fictive pressure structure to be recorded by the glass during the quench [63-64].
172 Therefore, the glass structure frozen-in after quenching is the structure recorded by the glass
173 under high-pressure conditions.

174 Recovered samples are optically checked for the presence of crystals. Most of the obtained
175 glasses were clear and transparent; however, several high-pressure samples exhibited
176 blackening coloration indicating the presence of graphite. This is a currently known
177 phenomenon during high-pressure piston-cylinder experiments [65-68]. The unavoidable
178 presence of carbon in the sample prior to the experiment (i.e. capsule walls, glass chips or
179 atmosphere) will reduce to graphite owing to the conditions that are not fully oxidising during
180 high-pressure talc-Pyrex experiment [69-71]. Nonetheless, the presence of graphite is suggested
181 not to affect the present results as C atoms are incorporated as free clusters in the glass voids.

182 ### 2.3 Scanning Electron Microscopy with Energy Dispersive X-ray Spectroscopy and Laser
183 Ablation Inductively Coupled Plasma Mass Spectrometry

184 Major elements quantification was performed on a Scanning Electron Microscope JEOL JSM
185 5800LV equipped with an SDD SAMx dispersive spectrometer (SEM-EDS, Institut des
186 Matériaux de Nantes Jean Rouxel, IMN). Analytical conditions were 15 kV for voltage and 0.5
187 nA for current. Acquisition were conducted on a 20 µm spot size in order to avoid Na loss under
188 the electron beam. We acquired five to ten scans of 60 s on each 1 atm. glass samples pre-
189 embedded in epoxy resin plug. The standards used for the different oxides are corundum for
190 Al_2O_3, wollastonite for SiO_2 and CaO, and NaCl for Na_2O.

191 The glass B_2O_3 content was determined using Laser Ablation Inductively Coupled Plasma Mass
192 Spectrometry (LA-ICP-MS, LPG) for providing more robust results than with the shortfall

obtained from SEM-EDS measurements. The spectrometer is an ArF excimer laser (193 nm, Analyte G2, Photon Machines) that is coupled to a quadrupole ICP-MS (Varian Bruker 820-MS). The ablations were performed in a HelEx II 2-Volume Cell with He as a carrier gas. We used a laser energy density of 4.54 $J.cm^{-2}$ with a repetition rate of 10 Hz. All the analyses were performed in a spot mode with a circular spot size of 110 µm in diameter. At least five acquisitions were performed on each glass sample. Acquisition time was set to 30 s with points collected every ~0.25 s (total number of points per analysis ~120), preceded and followed by a 30 s blank acquisition. We used the glasses investigated in Jolivet et al. [62] to calibrate the LA-ICP-MS signal: ISG, NH, LJ3 and LJ4 with 16.5, 15.1, 34.9 and 30.7 mol.% B_2O_3, respectively.

2.4 ^{11}B and ^{27}Al Solid State Nuclear Magnetic Resonance spectroscopy

^{11}B and ^{27}Al Solid State NMR was performed on a Bruker Avance III 500 MHz spectrometer (IMN) using a 2.5 mm Magic Angle Spinning (MAS) probe at the Larmor frequency of 160.46 and 130.32 MHz, respectively. The ^{11}B and ^{27}Al spectra are referenced against H_3BO_3 solution at 19.6 ppm and $Al(NO_3)_3$ solution at 0 ppm, respectively. The glass powders were loaded into ZrO_2 rotors with Teflon caps. The MAS frequency was set to 20 kHz for ^{11}B and 20 or 26 kHz for ^{27}Al depending on the presence of high-coordinated Al species. The recycle delay was set to 5 s for ^{11}B and 1 s for ^{27}Al. All MAS spectra were acquired with a radio frequency field strength of 20 kHz, and single pulse excitation of $\pi/12$ for both ^{11}B and ^{27}Al. Up to 512 and 2048 scans were collected for ^{11}B and ^{27}Al respectively. All ^{11}B spectra were processed prior to deconvolution for determining the N_4 parameter: first, the probe ^{11}B background signal is removed by subtracting an experimental spectrum of an empty rotor acquired at identical experimental conditions, and then the contribution of satellite transitions is removed from the central band, in accordance with the procedure described in Angeli et al. [2]. The ^{11}B 3Q-MAS spectra were acquired at a MAS frequency of 20 kHz and a recycle delay of 1 s. We used a 4

pulses sequence including Z filter. The 3Q excitation pulse length was 3.9 µs for a r.f. field of 140 kHz. For 3Q reconversion, we used a 12.5 µs (1/4 of the MAS period) divergent DFS (Double Frequency Sweep) pulse from 100 kHz to 1.5 MHz using a r.f. field strength of 130 kHz [72]. The ^{11}B SQ-DQ (Single Quantum - Double Quantum) homonuclear correlation spectra were acquired using the $BR2^1_2$ pulse scheme for dipolar recoupling [73]. The MAS frequency was set to 20 kHz and the recycle delay to 3 s. During recoupling we used π-pulse length of 50 µs corresponding to r.f. field of 10 kHz (i.e. half of the MAS frequency), as required for the $BR2^1_2$ scheme. The transmitter frequency (offset) was optimized to -6.7 ppm. We used a short excitation/reconversion time of 400 µs. Prior to DQ (t1) evolution, we used a π selective pulse of 8 µs sandwiched by two τ intervals of 21 µs in order to eliminate DQ coherences involving a single nucleus. τ (calculated according to ref. [74]) ensures rotor synchronization (the delay between the end of the excitation and the start of the conversion of DQ coherences is a multiple of the MAS period). Between 40 and 64 slices were acquired in the indirect dimension for which 128 or 192 scans were co-added, depending on the samples.

2.5 ^{11}B MAS NMR fitting protocol

Fitting the ^{11}B MAS NMR spectrum requires the combined knowledge of 1) the glass structure and 2) the interactions between nuclei. It is crucial to select the appropriate functions to accurately reproduce each boron environment. In other words, the shape of the fitting functions should be carefully chosen and optimized while considering all possible boron arrangements. This later point is still debated and there is only little agreement on ^{11}B MAS NMR spectrum fitting through the literature. For instance, it is difficult to find a well-described methodology for ^{11}B MAS NMR spectrum fitting as most authors do not go into too much details on this aspect. In the present study, we decided to follow the method presented in Angeli et al. [75] with minor adjustments to account for the differences in the chemical composition of the glasses.

In consistency with the literature data [2,75], we conducted the spectral decomposition with three or four components, using the DMfit software [76]. The effect of the EFG (Electric Field Gradient) distribution is well known and makes the line shape of quadrupolar nuclei asymmetrical. However, given the high symmetry of the boron environment in BO_4 units, the quadrupolar coupling constant (Cq, related to the EFG) is low [2,52,77], which induces that the line shape is almost symmetrical. Therefore, we used Gaussian line shape to reproduce the BO_4 environments that has been a commonly used solution for BO_4 fitting in previous works [41,62,78-81]. The BO_4 environment is a composition of several individual components for aluminoborosilicate glass compositions: BO_4-SiO_4 and BO_4-BO_3 bonding units [15,52,79,82]. It should be emphasised that BO_4-BO_4 and BO_4-AlO_4 bonds as well as NBO on BO_4 units are not energetically favoured [2,15,30,83-87]. The proportion of BO_4-SiO_4 and BO_4-BO_3 bonding units depends on the K' value. With high K' value, all BO_4 units should be surrounded by four SiO_4 units, and the corresponding signal should appear around -1 ppm in the ^{11}B MAS NMR spectra. The replacement of a SiO_4 unit by a BO_3 unit induces a shift to higher values in chemical shift of the BO_4 signal in the ^{11}B MAS NMR spectra [52,60,88-89]. A reliable way to determine the presence of BO_4-BO_3 bonding units is by performing ^{11}B SQ-DQ NMR acquisition that allows homonuclear correlations through a specific pulse sequence [74,82,90-91]. The obtained ^{11}B SQ-DQ spectra are provided in the Suppl. Mat. in Figure S1. The chemical shift (δ_{iso}) and the peak width (FWHM) corresponding to BO_4(3Si,1B) bonding units can be obtained from a fit of the projection of the 2D spectra selected slices on the 1Q dimension [52,92] (F2 axis, see Suppl. Mat. Figures S1 to S3). It should be pointed out that the presence of BO_4(2Si,2B) bonding unit is believed to be highly improbable given the relatively high K' values of the investigated glass compositions. The derived δ_{iso} and FWHM parameters obtained from fitting the 1Q projection are then used (and fixed) to fit the 1D spectra with a first Gaussian line. The presence of another contribution at lower δ_{iso} is then attributed to BO_4(4Si,0B)

bonding units that is reproduced with another Gaussian line. For Ca21B18-0, the decomposition protocol with Gaussian lines to account for the presence of several BO_4 units ended up with an unreliable fit due to the low intensity of the BO_4(4Si,0B) line. Therefore, we reproduced the BO_4 signal of Ca21B18-0 with a single Gaussian line. The parameter of this line turned out to be very close to the parameters of the BO_4(3Si,1B) component obtained from the ^{11}B DQ-SQ spectrum. Thus, almost all of the BO_4 units are BO_4(3Si,1B) units; although a low amount of BO_4(4Si,0B) should still be present in the glass structure. The BO_3 region is a combination of two components historically associated with BO_3 in ring and in non-ring configuration [52,58-59]. However, an increasing number of studies [14-15,93] investigating the interconnection between boron species through homonuclear correlations suggested that the denomination "BO_3 ring" and "BO_3 non-ring" appears not fully adapted. Therefore, we have chosen to use the terms "BO_3-1" and "BO_3-2" to represent the two BO_3 environments. This terminology is preferred since it is evident that there are multiple BO_3 environments; however, the exact geometrical configuration of each BO_3 environment remains unclear. The shape of these BO_3 is also a source of discussion. Various studies are fitted the BO_3 region with function simulating a distribution of the crystalline environment using a Gaussian distribution for each of the parameters δ_{iso}, Cq and η_q (the asymmetry parameter), which has proven effective in modelling this region, despite the lack of a true physical meaning [52,75,94]. As actually no better line shape has been established, we decided to use the Gaussian distribution of parameters. This is implemented as 'amorphous' line shape in the DMfit program [76]. This may not be the most accurate function but with appropriate fitting protocol, one can achieve to have comparable fits along the study. For that, the 1D spectra have been fitted in parallel to the 2D (3QMAS) spectra to ensure that the used parameters are consistent in both cases. The fitting of the 2D ^{11}B 3QMAS spectra obtained on the ambient pressure samples are presented in Figure S4 of the Suppl. Mat.. The η_q parameter has shown a limited influence on the fit results and was fixed to 0.2 for BO_3-

1 and 0 for BO_3-2, without distribution. Error on ^{11}B NMR fitting have been calculated using the Monte-Carlo method implemented in the DMfit program [76].

2.6 ^{27}Al MAS NMR fitting

The ^{27}Al NMR spectra have been fitted with up to three components corresponding to AlO_4, AlO_5 and AlO_6 species, around 60, 30 and 0 ppm, respectively. Precisely, Ca-bearing glass spectra have been fitted with 3 components, and Na-bearing glass spectra with only two as no AlO_6 was found in these samples. In order to take into account the EFG distribution for Al nuclei, we used Czjzek line shape [95-96] implemented (as the 'Cz simple' model) in the DMfit program [76]. The complete fitting protocol will not be presented here as extensive work have been performed previously on ^{27}Al solid-state NMR on amorphous solid [19,97-100].

3 Results

3.1 Ambient pressure ^{11}B MAS NMR spectra

^{11}B MAS NMR spectra for the four pristine (i.e. ambient pressure synthesis, -0) glasses are presented along with the fitted components (and the residual from the fit) in Figure 1, subtracted from the stator and first satellite transition signals [2,75-76]. The ^{11}B NMR spectra acquired at a 11.7 T magnetic field are characterised by a quasi-symmetric component centred around 0 ppm in chemical shift, corresponding to the tetrahedral BO_4 units that is partly overlapping with the asymmetric broad components corresponding to the planar triangles BO_3 units between ~-5 and 20 ppm. At first sight, the two sets of spectra for Na-bearing glasses (Figure 1A and 1C) show an intense BO_4 component as compared to the BO_3 signal; where the intensities are more balanced between BO_3 and BO_4 in the sets of spectra for Ca-bearing glasses (Figure 1B and 1D). This suggests that the proportion of BO_4 is higher in sodic compositions, as compared to calcic compositions, as was previously observed in the literature for similar glass systems [9,101]. We can also observe clear differences in the shape of the spectra, and more precisely

317 the line shape of the BO_3 region, varying as a function of the type and the content of modifier
318 cation in the glass, as was previously observed in the literature [91,101-103]. Considering the
319 variability in the BO_3 line shape as a function of glass composition, it appears difficult to
320 compare the line shape without relevant simulation of the BO_3 frequency region. However, it
321 seems at first sight that the proportion and line shape of the different BO_3 species signal are
322 also affected by the change in glass compositions, owing to the clear differences in the full BO_3
323 line shape frequency region.

324 3.2 ^{11}B MAS NMR spectra for samples synthesised under different pressure conditions

325 The ^{11}B MAS NMR spectra obtained from the glass synthesised at different pressures are
326 plotted in Figure 2. The spectra are normalised with respect to the area in the displayed figure
327 window. Therefore, the change in spectrum area in Figure 2 is directly related to the species
328 proportion change and therefore the N_4 value (see Table 2). We clearly observe in Figure 2 that
329 the BO_4 peak area increases and the BO_3 peak area decreases with pressure increase. It implies
330 that the N_4 increases with increasing pressure. This observation is in agreement with previously
331 observed changes in the glass structure with pressure [34-35,47,51,54-55]. However, it seems
332 that the change in spectrum area for Na22B23 is slower than for other samples. In Figure 2, we
333 also observe a different behaviour as a function of the type of modifier cation. For instance, in
334 Ca-bearing glass compositions (Figures 2B and 2D), the spectrum area change appears linear
335 with increasing pressure. Conversely, we do not observe the same behaviour for Na-bearing
336 compositions (Figures 2A and 2C). Whereas there is a clear difference in between the ambient
337 and the 2.0 GPa pressure spectra, the intermediate sample spectra (from 0.5 to 1.5 GPa) seem
338 to have nearly superimposable spectra suggesting the presence of a plateau in the boron
339 coordination for Na-bearing glass compositions. We observe this unexplained behaviour for
340 both Na22B23 and Na35B8 glass compositions suggesting that it is beyond any possible
341 analytical error.

4 Discussion

4.1 Rationale for boron speciation at ambient pressure: Comparison with available models.

The parameters derived from the fitted spectra in Figure 1 are provided in Table 2. The first striking feature is the similarity in the line shape of the BO_3-1 component for samples with the same modifier cation. In other words, the BO_3-1 for the Na22B23-0 sample (Figure 1A) is very similar to the BO_3-1 of the Na35B8-0 sample (Figure 1C); the BO_3-1 of the Ca21B18-0 sample (Figure 1B) is very similar to the BO_3-1 of the Ca33B11-0 sample (Figure 1D). In Table 2, we observe that the δ_{iso} values are comparable for a given modifying cation (Na or Ca) and are not affected by the changes in R' value: with 17.4 ppm for both Ca21B18-0 and Ca33B11-0, and about 18.5 ppm for both Na22B23-0 and Na35B8-0. This latter point appears to suggest that BO_3-1 local environment is more affected by the type of modifier cation present in the glass than by the change in R' value. On the other hand, the line shape of the BO_3-2 environment seems to be less affected by the type of modifying cation than by the change in R' value. The BO_3-1 is likely to be present in more depolymerized region of the glass (i.e. near modifier cations), whereas the BO_3-2 is possibly located in mixed regions with less contact with Na^+ and Ca^{2+} cations. However, we can observe a larger Cq and higher δ_{iso} for Na-bearing samples (>2700 kHz) than for Ca-bearing samples (~2600 kHz). The FWHM CS and FWHM Cq appear to vary more with R' than with the cation type. For instance, the FWHM Cq value changes from 350 to 900 kHz in between the Na22B23-0 (R' = 0.7) and Na35B8-0 (R' = 2.7).

As observed from the data in Table 2, the BO_4 derived parameters (i.e. position and width) are not affected neither by the change in modifier cation nor by the R' values. On the contrary, the proportion of BO_4 over total boron changes strongly as a function of the modifier cation. We explained this difference by the fact that BO_4 units require charge compensation with either Na^+ or Ca^{2+} in their close surrounding. Several studies have demonstrated that the proportion of BO_4 is maximized for Na-bearing glass compositions, and that the N_4 generally decreases with the

replacement of Na by another alkali or alkaline-earth cation [2,102-103]. A comparable behaviour is observed in the present study. For samples with near R' values (Na22B23-0 vs Ca21B18-0 and Na35B8-0 vs Ca33B11-0), the percentage of BO_4 in Ca-bearing glasses is roughly half the BO_4 percentage for Na-bearing glasses: 18% vs 41% for samples with low R'; 23% vs 47% for samples with high R'. A second information is the small change in the N_4 value when R' increases: from 41% to 47% for the Na-bearing samples; from 18% to 23% for the Ca-bearing ones. This was already observed for a large range of compositions [16,18,92] and was predicted by different structural models [8,17]. For comparison, the N_4 values obtained with two models [8,104] are provided in Table 3 along with the corresponding measured N_4. The Du and Stebbins [8] model is based on the Dell model [17], and on multiple observations in the SiO_2-Al_2O_3-B_2O_3-K_2O/CaO system and does not take into consideration the effectiveness of the charge compensation cations. Therefore, the model is not fully adapted to predict the N_4 for the Ca21B18-0 and Ca33B11-0 samples: 64% predicted versus 18% measured and 56% predicted versus 23% measured; respectively. For Na-bearing glass compositions, the calculated N_4 is in better agreement with the measured N_4 by ^{11}B MAS NMR: 61% predicted against 41% measured for Na22B23-0, and 54% predicted and 47% measured for Na35B8-0.

On the other hand, the study from Lu and co-authors [104] is based on analytical modelling over a large range of glass compositions. This led to the development of several models to interpret the glass structure from the glass major element composition. The model is based on R' and K' values with modified coefficients to consider: 1- Priority for charge compensation of the network former units; and 2- Capacity of charge compensation of the modifier alkali and alkaline-earth. It results in a better prediction of the N_4 values as observed in Table 3. The N_4 value prediction for low R' is close to the measured value: 24% predicted against 18% measured for Ca21B18-0, 45% predicted against 41% measured for Na22B23-0; however, the model fails to reproduce the measured N_4 values for high R' glasses: 46% predicted against 23% measured

for Ca33B11-0, 59% predicted against 47% measured for Na35B8-0. The results reveal notable differences between current models and the observed behaviour of boron speciation in these simple glass systems. Therefore, further development is required to make precise predictions of tetrahedral boron content, even for relatively simplistic compositions.

4.2 Effect of pressure conditions on ^{11}B NMR spectra and boron coordination

Pressure increase does not drastically change the line shape of the spectra suggesting a small variation in the fit parameters. Nevertheless, a closer look at Figure 2B and 2C suggests that pressure is not affecting both BO_3-1 and BO_3-2 the same way. The effect of pressure in the BO_4 region is somehow as subtle as for the BO_3. We observe a small shift of the maximum toward lower chemical shift for all samples. This shift has already been documented and has been attributed to an increase in the proportion of BO_4(4Si) with increasing pressure [56,105]. This behaviour is induced by the decrease in the proportion of BO_3 and the avoidance between BO_4 tetrahedra [2,15,30], which makes SiO_4 the available unit to link with.

We propagated the obtained fits for ambient pressure sample spectra to the spectra obtained for the high-pressure samples. The parameters were fixed for all components except for BO_4(4Si) species. During the fitting, only the peak intensities were allowed to vary. The results are shown in Figure 3 for the 2.0 GPa samples (the results for the fitting of the 3QMAS spectra are available in Suppl. Mat. in Figure S4 and S5). The derived parameters are provided in Table 2. As seen in Figure 3, the fit parameters reproduce adequately the spectra at 2.0 GPa with only little imperfections.

The N_4 for all samples is calculated from results shown in Table 2 and plotted in Figure 4 as a function of pressure. The first evident feature in Figure 4 is the higher N_4 values for Na-bearing samples as compared to Ca-bearing ones, regardless of the pressure conditions. This reflects the higher capacity for Na^+ cations to compensate the excess negative charge on BO_4 units

[2,102-103]. As observed for the ambient pressure glasses, the samples with high R' values exhibit higher N_4 value as compared to samples with low R' values, again regardless of the pressure conditions. Whereas both types of glass compositions (Na- and Ca-bearing) have similar evolution with respect to the N_4, we observe a clear difference in the evolution of the N_4 with pressure as function of the type of the modifier cation. For Ca-bearing samples, the N_4 evolution is almost linear with pressure and is consistent with the spectrum line shape evolution shown in Figure 2. The N_4 value at 2 GPa is almost twice the N_4 value determined for ambient pressure glasses, regardless of R' value. The difference in the N_4 values for low R' glasses and the high R' glasses is very small: 18% against 23% for Ca21B18 and Ca33B11 respectively for ambient pressure samples; and is almost constant with pressure increase: 37% against 44%, respectively at 2 GPa.

On the other hand, for Na-bearing samples, we observe a clear step with almost constant N_4 for samples recovered from 0.5, 1, and 1.5 GPa, regardless of R' value. This was suspected from the spectrum comparison in Figure 2. Looking at the literature, there is no study that showed this behaviour. However, Smedskjaer and co-authors [33], who studied the evolution of the N_4 in mixed alkali-alkaline-earth borate glasses (Na_2O-CaO-B_2O_3), reported a linear evolution of the N_4 from ambient to 0.5 GPa, and a slowdown of the trend at 0.6 GPa. Several phenomena could be at the origin of the plateau observed for Na22B23 and Na35B8, from a "simple" resistance of the glass to pressure ranging from 0.5 to 1.5 GPa, to a more complex structural adaptation to pressure without modification of the BO_4 proportion. On the contrary to Ca-bearing samples, we observe a strong difference in the N_4 behaviour for Na-bearing samples depending on R'. Between ambient pressure and 2.0 GPa, the N_4 value ranges from 41% to 48% for glasses with low R' value (Na22B23) and ranges from 47% to 71% for glasses with high R' values (Na35B8). As shown below, the glass structure is highly polymerised for low R' Na-bearing samples (i.e. not enough Na^+ cations for forming NBOs) and does not favour the

441 conversion of BO_3 to BO_4. The Na35B8 glass samples have initially much more Na^+ cations
442 that are available for the conversion of BO_3 into BO_4 units. With further pressure increase
443 (above 2 GPa), it has been shown that the N_4 value continues to increase [35,51,53]. However,
444 as we showed for the Na22B23 series, the pressure effect will be modulated by the capacity of
445 the structure (i.e. the available NBO…Na^+ that could be broken to charge compensate the BO_3
446 to BO_4 transformation).

447 We plot in Figure 5 the variation in the percentage of each structural unit as a function of
448 pressure. For each series, the four identified components are plotted along with the
449 corresponding N_4 values, except for the Ca21B18 series where the N_4 is directly extracted from
450 the unique BO_4 component. In Figure 5, we show that 1) the percentage of the BO_3-1 component
451 is always decreasing and 2) the percentage of the BO_4(4Si) component is always increasing
452 regardless of the glass composition (Ca21B18 seems to make an exception). As mentioned
453 previously, this increase in BO_4(4Si) component is likely to result from the general increase of
454 the BO_4 and decrease of the BO_3 percentages. It would imply that globally less BO_4-BO_3 bonds
455 are probable with increasing pressure and by extension less BO_4(3Si,1B). If we compare how
456 the BO_4 components are increasing at the expense of the BO_3 with sodium or calcium, we
457 observe two distinct behaviours. For Ca-bearing samples, we observe a systematic increase in
458 the BO_4(3Si,1B) percentage with a balanced consumption of BO_3-1 and BO_3-2 for low-R'
459 series, and a major decrease in the BO_3-1 percentage for high-R' series. For Na-bearing
460 samples, the N_4 increase seems to be related to the increase in the BO_4(4Si) percentage
461 accompanied by a decrease in the BO_3-1 unit. We observe that BO_3-2 species remain almost
462 constant at pressure $\geq$ 0.5 GPa. Except for Na35B8 samples, the SQ-DQ spectra did not reveal
463 the presence of BO_4-BO_4 correlations (see Suppl. Mat. Figure S1). The spectrum comparison
464 between the Na35B8 glasses at ambient pressure and 2.0 GPa showed the presence of BO_4-BO_4
465 correlations at the expense of BO_3-BO_3 units, which is not seen in any other glass series.

4.3 Effect of pressure: Evolution of the aluminium environment

The general behaviour of cations under compression is an increase in their coordination number, and aluminium does not make exception [42-48]. Many studies focussed on the change in the aluminium environment in glass under extreme conditions (i.e. pressure), and revealed that AlO_4 network former units are reorganised into AlO_5 and AlO_6 units [8,45,47,55,106-107]. From the literature, two interesting features are noteworthy for our study. First of all, the role of AlO_5 and AlO_6 is very debated, molecular dynamics simulations suggest that they are even less prone to coordinate NBO than AlO_4 [22-24]. As those species most likely require less charge-compensation by the electropositive network modifiers [23,108-109], the Na^+ and Ca^{2+} present on the AlO_4 are then liberated conjointly with the Al coordination number increase. Secondly, as mentioned before for boron, in Na-rich glasses, AlO_4 is very stable and the evolution of the average Al coordination number with pressure is much slower that in alkaline-earth glasses [6-7,45,49,108,110-111].

The calculated average coordination number calculated from ^{27}Al fit is displayed in Table 3, along with the calculated fraction of AlO_4 in the glass ($[AlO_4] = {}^4Al \times 2 \times [Al_2O_3]$ where ^4Al is the proportion of AlO_4 obtained from fit). A fit for ambient pressure glass samples is shown in Figure S6, and a synthetic table of the fitting parameters is presented in Table S7 both in the Suppl. Mat.. We observe that the average coordination number (Al_{CN}) is greater for Ca-bearing than for Na-bearing sample both for ambient pressure and high-pressure. In details, it appears that high R' glasses (i.e. Na35B8 and Ca33B11) have a faster increase in the average Al_{CN} with pressure, although the increase is limited for Na-bearing glass compositions. This behaviour was expected as sodium tends to stabilize tetrahedral units.

4.4 Changes in the glass polymerisation as a function of pressure

The measured BO_4 and AlO_4 units in glasses are the only species requiring charge compensation by available Na^+ or Ca^{2+} cations. The excess modifier cations (Na^+ and Ca^{2+}) disrupts the glass structure to form NBOs and thus decreases the glass polymerisation. The NBO per formula unit formed with these excess cations is calculated with the following equation:

$$[NBO] = 2 \times ([Na_2O] + [CaO]) - [AlO_4] - [BO_4] \qquad (1)$$

The results are provided in Table 3. We plot in Figure 6 the calculated NBO per formula unit as a function of mol.% BO_4 corresponding to the network forming unit requiring charge compensation. We identified two cases: either there is only conversion from BO_3 to BO_4 unit, Na^+ or Ca^{2+} are scavenged from NBO sites (in the vicinity of BO_3 species) and the trend slope will be close to -1; or part of the charge compensating cations involved in the conversion from BO_3 to BO_4 unit are also coming from the conversion of AlO_4 to AlO_5 unit implying the release of Na^+ or Ca^{2+} cation and the trend slope will be higher than -1.

In Figure 6, the glass compositions with high R' value (Na35B8 and Ca33B11) are lying on the upper part of the plot (i.e. high NBO concentration) whereas the glass compositions with low R' value (Na22B23 and Ca21B18) are on the bottom part of the plot (i.e. low NBO concentration). The Na22B23 glass series exhibits a very small dispersion on the mol.% BO_4 and a slope of -0.95. This glass composition is the most polymerised with high N_4 value at ambient pressure and only a few NBO available; explaining its position at the bottom right of Figure 6. However, as mentioned earlier, the N_4 increase for this series is limited (from 41% to 48% between ambient and 2.0 GPa pressure). As observed from Table 3, the change in the Al_{CN} is very low with increasing pressure for Na-bearing glass compositions. It implies that almost no charge compensator is released from the AlO_4 to AlO_5 transformation and Na^+ cations stay as charge compensators for AlO_4 units with increasing pressure. From those considerations, the

increase in the N_4 value with increasing pressure is only due to the scavenging of Na^+ cations associated to NBOs.

By opposition, for Ca33B11 glass series (slope near -0.5) there is a release of charge compensators from AlO_4 units that convert into AlO_5 units. The Ca^{2+} release partly compensates the conversion from BO_3 to BO_4 units. In addition, it also points out that half of the Ca^{2+} used for the charge compensation of the newly formed BO_4 units is coming from NBO sites. The second half is released from AlO_4 units converted into AlO_5 units.. As described before, the AlO_4 compensation by alkaline-earth cations is not very efficient and a non-negligible proportion of AlO_5 (to a lesser extent AlO_6) is identified in the ambient pressure glass. The pressure increase will further favour the AlO_4 to AlO_5 and AlO_6 promotion for Ca33B11 glasses. Surprisingly, this mechanism does not seem to apply for the Ca21B18 glass series showing a slope of -0.87. It indicates that more NBOs are used to compensate for the formation of BO_4 from BO_3 species. Thus, the conversion from AlO_4 to AlO_5 and the accompanied Ca^{2+} release does not seem to be efficient. This behaviour is somewhat unexpected given that the Ca21B18 glass series has fewer NBOs available than the Ca33B11 series.

The method used to represent the evolution of BO_4 content as a function of the NBO content when pressure is increased is similar to that proposed by Bista and co-authors [34-35], who plotted the proportion of AlO_4 against the proportion of BO_4. In their representation, a -1 slope indicates that the cations released by the transformation of AlO_4 to AlO_5 with pressure are completely compensating for the formation of BO_4. The slope becomes steeper when the formation of BO_4 is slower than the decrease of the AlO_4 content. This indicates that the released cations are available to form NBOs. However, representing a species against the NBO content makes it more general. This approach can be applied to other cationic species, such as Mg^{2+}, Zr^{4+}, or $Fe^{2+/3+}$, which may also undergo significant modifications under pressure [112-115].

4.5 Implications for aluminoborosilicate glass properties

The results presented here display a global decrease of the NBO per formula unit, pointing towards an increase in the glass polymerization with increasing pressure. This behaviour is explained by the conversion of BO_3 into BO_4 species being faster than the AlO_4 to AlO_5 and AlO_6 conversion. Indeed, as the first phenomena is "consuming" NBO (for charge compensation), and the second is releasing modifying cations, the extent of one over the other is the main driver for polymerisation or depolymerisation upon pressure. The observed increase in N_4 value with increasing pressure has been shown by previous studies [34-38,47,51-53,55]. For the purpose of nuclear matrix durability, the increase in N_4 is beneficial as it corresponds to a decrease in the NBO proportion and thus to an increase in the glass polymerisation [36,53]. However, we show that the behaviour is not the same depending on the type of cation involved. For instance, in the case of Ca-bearing glasses we show that the N_4 increase is compensated by Ca coming from the NBO sites. It is thus possible to define a precise starting chemical composition in order to obtain specific properties after synthesis at high-pressure. Structural properties tuning with pressure can be of great interest in the case of nuclear waste immobilisation in glasses.

Most of the studies we have conducted recently focused on the incorporation of halogens and merely addressed the combined effect of pressure and volatile dissolution in the glass [40-41]. In fact, both parameters are affecting the glass structure. Morizet and co-authors [39,57] demonstrated that there is gradual decrease in the NBO concentration with the incorporation of iodine at constant pressure. Therefore, the combined effect: pressure increase and volatile incorporation; could induce an even better durability for aluminoborosilicate glass. It remains to be determined whether both effects will combine or one will dominate. Nevertheless, the present study provides a strong basis for future work on the volatile dissolution mechanisms and impact on glass structure, as it extends the range of acceptable glass compositions for

562 nuclear waste incorporation (actually limited to: B_2O_3 < 15 mol.%, SiO_2 ~50 mol.%, Al_2O_3 ~5-
563 10 mol.%, Na_2O+CaO ~30 mol.%).

564 ## 5 Conclusion

565 Two series of aluminoborosilicate glass containing either Ca or Na were synthesized under
566 variable pressure conditions (ambient to 2.0 GPa) and characterized by ^{11}B and ^{27}Al solid-state
567 NMR. The effects of pressure and modifier cation (Ca or Na) as well as changes in R' value
568 were investigated. We modelled ^{11}B spectra using up to four components corresponding to BO_3-
569 1, BO_3-2, BO_4(1B,3Si), and BO_4(4Si), and we successfully propagated the fit from the ambient
570 pressure to the high-pressure samples. The calculated N_4 higher in Na-bearing than Ca-bearing
571 samples suggests that Na^+ is a better cation than Ca^{2+} for compensating the negative charge on
572 BO_4 units, regardless of the pressure. The proportion of BO_4 in Ca-bearing glasses increases
573 linearly with pressure, reaching twice the amount at 2 GPa compared to atmospheric pressure.
574 In Na-bearing glasses, a not-yet explained plateau of N_4 values is observed between 0.5 and 1.5
575 GPa, probably induced by a resistance of the glass for reorganisation at such pressure range.
576 For glasses with similar modifier cations, it was observed that samples with high R' values had
577 a higher N_4 compared to samples with low R' values, regardless of the pressure. The percentage
578 of BO_4(4Si) always increases with pressure, which is consistent with previous studies. The
579 evolution of the components suggests that pressure is affecting BO_3-1 and BO_3-2 differently.
580 BO_3-1 may be present in more depolymerized regions near modifier cations, while BO_3-2 may
581 be present in mixed regions, possibly less in the direct environment of Na^+ and Ca^{2+} cations.
582 The ^{27}Al NMR analysis revealed that Na greatly stabilises AlO_4, and that the average
583 coordination number remains relatively constant with pressure in these glasses. However, Ca-
584 bearing samples exhibit a higher proportion of highly coordinated Al^{3+} cations, and the average
585 coordination number increases more significantly in Ca-bearing glasses. These findings are
586 discussed in terms of the proportion of NBO per formula unit, which decreases as pressure

increases. This is of significant interest in the production of durable materials such as nuclear waste glasses.

Acknowledgments

The authors are grateful to the Agence Nationale de la Recherche, which financed the current work through the ANR project "Iodine-CLEAN-UP" (ANR-20-CE08-0018). The authors thank the Région Pays de la Loire for funding the present research through the "Trajectoire nationale de la recherche ligérienne" program. The authors thank the Laboratoire de Planétologie et Géosciences. Solid State NMR and SEM/EDS measurements were performed on IMN's equipment platform, PLASSMAT, Nantes, France. The authors would like to thank N. Stephant (SEM/EDS) for the measurements.

References

[1] Holland D, Parkinson B, Islam M, Duddridge A, Roderick J, Howes A, et al. NMR insights into wasteforms for the vitrification of high-level nuclear waste. Applied Magnetic Resonance. 2007;32(4) :483-497.

[2] Angeli F, Charpentier T, De Ligny D, Cailleteau C. Boron speciation in soda-lime borosilicate glasses containing zirconium. Journal of the American Ceramic Society. 2010;93(9) :2693-2704.

[3] Gin S, Abdelouas A, Criscenti LJ, Ebert WL, Ferrand K, Geisler T, et al. An international initiative on long-term behavior of high-level nuclear waste glass. Materials Today. 2013;16(6) :243-248.

[4] Riley BJ, Schweiger MJ, Kim DS, Lukens Jr WW, Williams BD, Iovin C, et al. Iodine solubility in a low-activity waste borosilicate glass at 1000C. Journal of Nuclear Materials. 2014;452(1-3) :178-188.

[5] Riley BJ, Vienna JD, Strachan DM, McCloy JS, Jerden Jr JL. Materials and processes for the effective capture and immobilization of radioiodine: a review. Journal of Nuclear Materials. 2016;470 :307-326.

[6] Bunker BC, Kirkpatrick RJ, Brow RK. Local structure of alkaline-Earth boroaluminate crystals and glasses: I, Crystal chemical concepts-Structural predictions and comparisons to known crystal structures. Journal of the American Ceramic Society. 1991;74(6) :1425-1429.

[7] Bunker BC, Kirkpatrick RJ, Brow RK, Turner GL, Nelson C. Local structure of alkaline-earth boroaluminate crystals and glasses: II, ^{11}B and ^{27}Al MAS NMR spectroscopy of alkaline-earth boroaluminate glasses. Journal of the American Ceramic Society. 1991;74(6) :1430-1438.

[8] Du LS, Stebbins JF. Network connectivity in aluminoborosilicate glasses: A high-resolution ^{11}B, ^{27}Al and ^{17}O NMR study. Journal of Non-Crystalline Solids. 2005;351(43-45) :3508-3520.

[9] Quintas A, Caurant D, Majérus O, Charpentier T, Dussossoy JL. Effect of the nature of alkali and alkaline-earth oxides on the structure and crystallization of an aluminoborosilicate glass developed to immobilize highly concentrated nuclear waste solutions. 2009. arXiv preprint arXiv :09121576.

[10] Goel A, McCloy JS, Fox KM, Leslie CJ, Riley BJ, Rodriguez CP, et al. Structural analysis of some sodium and alumina rich high-level nuclear waste glasses. Journal of non-crystalline solids. 2012;358(3) :674-679.

[11] Collin M, Fournier M, Frugier P, Charpentier T, Moskura M, Deng L, et al. Structure of International Simple Glass and properties of passivating layer formed in circumneutral pH conditions. npj Materials Degradation. 2018;2(1) :4.

[12] Angeli F, Charpentier T, Jollivet P, de Ligny D, Bergler M, Veber A, et al. Effect of thermally induced structural disorder on the chemical durability of International Simple Glass. npj Materials Degradation. 2018;2(1) :31.

[13] Charpentier T, Martel L, Mir AH, Somers J, Jégou C, Peuget S. Self-healing capacity of nuclear glass observed by NMR spectroscopy. Scientific Reports. 2016;6(1) :25499.

[14] Yu Y, Keil P, Hansen MR, Edén M. Improved magnetization transfers among quadrupolar nuclei in two-dimensional homonuclear correlation NMR experiments applied to inorganic network structures. Molecules. 2020;25(2) :337.

[15] Lv, P., Stevensson, B., Yu, Y., Wang, T., & Edén, M. BO_3/BO_4 Intermixing in Borosilicate Glass Networks Probed by Double-Quantum ^{11}B NMR: What Factors Govern BO_4–BO_4 Formation?. *The Journal of Physical Chemistry C*. 2023 ;*127*(40), 20026-20040.

[16] Yun Y, Bray P. Nuclear magnetic resonance studies of the glasses in the system Na_2O-B_2O_3-SiO_2. Journal of NonCrystalline Solids. 1978;27(3) :363-380.

[17] Dell W, Bray P, Xiao S. ^{11}B NMR studies and structural modeling of Na_2O-B_2O_3-SiO_2 glasses of high soda content. Journal of Non-Crystalline Solids. 1983;58(1) :1-16.

[18] Zhong J, Bray PJ. Change in boron coordination in alkali borate glasses, and mixed alkali effects, as elucidated by NMR. Journal of non-crystalline solids. 1989;111(1) :67-76.

[19] Eden, M. (2020). Update on ^{27}Al NMR studies of aluminosilicate glasses. In Annual reports on NMR spectroscopy (Vol. 101, pp. 285-410). Academic Press.

[20] Mysen, B. O., Virgo, D., & Scarfe, C. M. (1980). Relations between the anionic structure and viscosity of silicate melts—a Raman spectroscopic study. American Mineralogist, 65(7-8), 690-710.

[21] Mysen, B. O., Virgo, D., & Kushiro, I. (1981). The structural role of aluminum in silicate melts—a Raman spectroscopic study at 1 atmosphere. American Mineralogist, 66(7-8), 678-701.

[22] Lee, S. K., & Sung, S. (2008). The effect of network-modifying cations on the structure and disorder in peralkaline Ca–Na aluminosilicate glasses: O-17 3QMAS NMR study. Chemical Geology, 256(3-4), 326-333.

[23] Okhotnikov K, Stevensson B, & Edén M. New interatomic potential parameters for molecular dynamics simulations of rare-earth (RE= La, Y, Lu, Sc) aluminosilicate glass structures: exploration of RE^{3+} field-strength effects. Physical Chemistry Chemical Physics. 2013;15(36), 15041-15055.

[24] Stevensson, B., Jaworski, A., & Edén, M. (2017). The structural roles of Sc and Y in aluminosilicate glasses probed by molecular dynamics simulations. Journal of Non-Crystalline Solids, 460, 36-46.

[25] Charpentier T, Okhotnikov K, Novikov AN, Hennet L, Fischer HE, Neuville DR, & Florian P. Structure of strontium aluminosilicate glasses from molecular dynamics simulation,

neutron diffraction, and nuclear magnetic resonance studies. The Journal of Physical Chemistry B. 2018;122(41), 9567-9583.

[26] Jaworski, A., Stevensson, B., & Edén, M. (2016). The bearings from rare-earth (RE= La, Lu, Sc, Y) cations on the oxygen environments in aluminosilicate glasses: a study by solid-state ^{17}O NMR, molecular dynamics simulations, and DFT calculations. The Journal of Physical Chemistry C, 120(24), 13181-13198.

[27] Feil D, Feller S. The density of sodium borosilicate glasses related to atomic arrangements. Journal of non-crystalline solids. 1990;119(1) :103-111.

[28] Yoshida S, Hayashi Y, Konno A, Sugawara T, Miura Y, Matsuoka J. Indentation induced densification of sodium borate glasses. Physics and Chemistry of Glasses-European Journal of Glass Science and Technology Part B. 2009;50(1) :63- 70.

[29] Kato Y, Yamazaki H, Yoshida S, Matsuoka J. Effect of densification on crack initiation under Vickers indentation test. Journal of Non-Crystalline Solids. 2010;356(35-36) :1768-1773.

[30] Smedskjaer MM, Mauro JC, Youngman RE, Hogue CL, Potuzak M, Yue Y. Topological principles of borosilicate glass chemistry. The Journal of Physical Chemistry B. 2011;115(44) :12930-12946.

[31] Barlet M, Delaye JM, Charpentier T, Gennisson M, Bonamy D, Rouxel T, et al. Hardness and toughness of sodium borosilicate glasses via Vickers's indentations. Journal of Non-Crystalline Solids. 2015;417 :66-79.

[32] Wondraczek L, Sen S, Behrens H, Youngman RE. Structure-energy map of alkali borosilicate glasses: Effects of pressure and temperature. Physical review B. 2007;76(1) :014202.

[33] Smedskjaer MM, Youngman RE, Striepe S, Potuzak M, Bauer U, Deubener J, et al. Irreversibility of pressure induced boron speciation change in glass. Scientific reports. 2014;4(1) :1-6.

[34] Bista S, Morin EI, Stebbins JF. Response of complex networks to compression: Ca, La, and Y aluminoborosilicate glasses formed from liquids at 1 to 3 GPa pressures. The Journal of Chemical Physics. 2016;144(4) :044502.

[35] Bista S, Stebbins JF, Wu J, Gross TM. Structural changes in calcium aluminoborosilicate glasses recovered from pressures of 1.5 to 3 GPa: Interactions of two network species with coordination number increases. Journal of NonCrystalline Solids. 2017;478 :50-57.

[36] Lee AC, Kim EJ, Lee SK. Pressure-induced structural evolution in boron-bearing model rhyolitic glasses under compression: Implications for boron isotope compositions and properties of deep melts in Earth's interior. Geochimica et Cosmochimica Acta. 2022;332 :220-238.

[37] Cicconi MR, Pili E, Grousset L, Florian P, Bouillard JC, Vantelon D, et al. Iodine solubility and speciation in glasses. Scientific reports. 2019;9(1) :1-13.

[38] Jolivet V, Morizet Y, Paris M, Suzuki-Muresan T. High pressure experimental study on iodine solution mechanisms in nuclear waste glasses. Journal of Nuclear Materials. 2020 :152112.

[39] Morizet Y, Jolivet V, Trcera N, Suzuki-Muresan T, Hamon J. Iodine local environment in high pressure borosilicate glasses: An X-ray photoelectron spectroscopy and X-ray absorption spectroscopy investigation. Journal of Nuclear Materials. 2021;553 :153050.

[40] Jolivet V, Morizet Y, Trcera N, Fernandez V, Suzuki-Muresan T. Incorporation of chlorine in nuclear waste glasses using high-pressure vitrification: Solubility, speciation, and local environment of chlorine. American Mineralogist. 2023;108(6) :1032-1042.

[41] Soudani S, Paris M, Morizet Y. The effect of iodine on the local environment of network-forming elements in aluminoborosilicate glasses: An NMR study. *J Am Ceram Soc*. 2024; 107: 4557–4571.

[42] Mysen BO. Effect of pressure, temperature, and bulk composition on the structure and species distribution in depolymerized alkali aluminosilicate melts and quenched melts. Journal of Geophysical Research: Solid Earth. 1990;95(B10) :15733-15744.

[43] Yarger JL, Smith K, Nieman RA, Diefenbacher J, Wolf GH, Poe BT, et al. Al coordination changes in high-pressure aluminosilicate liquids. Science. 1995;270(5244) :1964-1967.

[44] Poe BT, Romano C, Zotov N, Cibin G, Marcelli A. Compression mechanisms in aluminosilicate melts: Raman and XANES spectroscopy of glasses quenched from pressures up to 10 GPa. Chemical Geology. 2001;174(1-3) :21-31.

[45] Allwardt JR, Stebbins JF, Schmidt BC, Frost DJ, Withers AC, Hirschmann MM. Aluminum coordination and the densification of high-pressure aluminosilicate glasses. American Mineralogist. 2005;90(7) :1218-1222.

[46] Allwardt JR, Poe BT, Stebbins JF. The effect of fictive temperature on Al coordination in high-pressure (10 GPa) sodium aluminosilicate glasses. American Mineralogist. 2005;90(8-9) :1453-1457.

[47] Lee SK, Mibe K, Fei Y, Cody GD, Mysen BO. Structure of B_2O_3 glass at high pressure: a B11 solid-state NMR study. Physical review letters. 2005;94(16) :165507.

[48] Lee SK, Sung S. The effect of network-modifying cations on the structure and disorder in peralkaline Ca-Na aluminosilicate glasses: O-17 3QMAS NMR study. Chemical Geology. 2008;256(3-4) :326-333.

[49] Kelsey KE, Stebbins JF, Singer DM, Brown Jr GE, Mosenfelder JL, Asimow PD. Cation field strength effects on high pressure aluminosilicate glass structure: Multinuclear NMR and La XAFS results. Geochimica et Cosmochimica Acta. 2009;73(13) :3914-3933.

[50] Lee SK, Kim YH, Chow P, Xiao Y, Ji C, Shen G. Amorphous boron oxide at megabar pressures via inelastic X-ray scattering. Proceedings of the National Academy of Sciences. 2018;115(23) :5855-5860.

[51] Lee SK, Lee AC, Kweon JJ. Probing medium-range order in oxide glasses at high pressure. The Journal of Physical Chemistry Letters. 2021;12(4) :1330-1338.

[52] Du LS, Stebbins JF. Solid-state NMR study of metastable immiscibility in alkali borosilicate glasses. Journal of noncrystalline solids. 2003;315(3) :239-255.

[53] Du LS, Allwardt J, Schmidt B, Stebbins J. Pressure-induced structural changes in a borosilicate glass-forming liquid: boron coordination, non-bridging oxygens, and network ordering. Journal of Non-Crystalline Solids. 2004;337(2) :196- 200.

[54] Wu J, Deubener J, Stebbins JF, Grygarova L, Behrens H, Wondraczek L, et al. Structural response of a highly viscous aluminoborosilicate melt to isotropic and anisotropic compressions. The Journal of Chemical Physics. 2009;131(10).

[55] Lee SK. Effect of pressure on structure of oxide glasses at high pressure: Insights from solid-state NMR of quadrupolar nuclides. Solid State Nuclear Magnetic Resonance. 2010;38(2) :45-57.

[56] Edwards T, Endo T, Walton JH, Sen S. Observation of the transition state for pressure-induced BO_3? BO_4 conversion in glass. Science. 2014;345(6200) :1027-1029.

[57] Morizet Y, Soudani S, Hamon J, Paris M, La C, Gautron E. IODINE DISSOLUTION MECHANISMS IN HIGHPRESSURE ALUMINOBOROSILICATE GLASSES AND ITS RELATIONSHIP TO OXYGEN SPECIATION. Journal of Materials Chemistry A. 2023.

[58] Jellison Jr G, Bray P. A structural interpretation of ^{10}B and ^{11}B NMR spectra in sodium borate glasses. Journal of Non-Crystalline Solids. 1978;29(2) :187-206.

[59] Sen S, Xu Z, Stebbins J. Temperature dependent structural changes in borate, borosilicate and boroaluminate liquids: high-resolution ^{11}B, ^{29}Si and ^{27}Al NMR studies. Journal of Non-Crystalline Solids. 1998;226(1-2) :29-40.

[60] Du LS, Stebbins JF. Nature of silicon- boron mixing in sodium borosilicate glasses: a high-resolution ^{11}B and ^{17}O NMR study. The Journal of Physical Chemistry B. 2003;107(37) :10063-10076.

[61] Morizet, Y., Paris, M., Hamon, J., La, C., Grolleau, S., & Suzuki-Muresan, T. Predicting iodine solubility at high pressure in borosilicate nuclear waste glasses using optical basicity: an experimental study. Journal of Materials Science. 2022; 57(35), 16600-16618.

[62] Jolivet V, Jossé L, Rivoal M, Paris M, Morizet Y, La C, et al. Quantification of boron in aluminoborosilicate glasses using Raman and ^{11}B NMR. Journal of Non-Crystalline Solids. 2019;511 :50-61.

[63] Bista S, Stebbins JF, Hankins WB, Sisson TW. Aluminosilicate melts and glasses at 1 to 3 GPa: Temperature and pressure effects on recovered structural and density changes. American Mineralogist. 2015;100(10) :2298-2307.

[64] Gaudio SJ, Lesher CE, Maekawa H, & Sen S. Linking high-pressure structure and density of albite liquid near the glass transition. Geochimica et Cosmochimica Acta. 2015;157, 28-38.

[65] Brooker R, Holloway JR, Hervig R. Reduction in piston-cylinder experiments: The detection of carbon infiltration into platinum capsules. American Mineralogist. 1998;83(9-10) :985-994.

[66] Brooker R, Kohn S, Holloway J, McMillan P, Carroll M. Solubility, speciation and dissolution mechanisms for CO_2 in melts on the $NaAlO_2$-SiO_2 join. Geochimica et Cosmochimica Acta. 1999;63(21) :3549-3565.

[67] Stamper C, Melekhova E, Blundy J, Arculus R, Humphreys M, Brooker R. Oxidised phase relations of a primitive basalt from Grenada, Lesser Antilles. Contributions to Mineralogy and Petrology. 2014;167 :1-20.

[68] Matjuschkin V, Brooker RA, Tattitch B, Blundy JD, Stamper CC. Control and monitoring of oxygen fugacity in piston cylinder experiments. Contributions to Mineralogy and Petrology. 2015;169 :1-16.

[69] Kagi R, Muntener O, Ulmer P, Ottolini L. Piston-cylinder experiments on H_2O undersaturated Fe-bearing systems: An experimental setup approaching fO_2 conditions of natural calc-alkaline magmas. American Mineralogist. 2005;90(4) :708-717.

[70] Morizet Y, Paris M, Sifre D, Di Carlo I, Ory S, Gaillard F. Towards the reconciliation of viscosity change and CO_2 induced polymerization in silicate melts. Chemical Geology. 2017;458 :38-47.

[71] Larre C, Morizet Y, Guillot-Deudon C, Baron F, Mangold N. Quantitative Raman calibration of sulfate-bearing polymineralic mixtures: A S quantification in sedimentary rocks on Mars. Mineralogical Magazine. 2019;83(1) :57-69.

[72] Kentgens A, Verhagen R. Advantages of double frequency sweeps in static, MAS and MQMAS NMR of spin I= 3/2 nuclei. Chemical Physics Letters. 1999;300(3-4) :435-443.

[73] Wang Q, Hu B, Lafon O, Trébosc J, Deng F, Amoureux JP. Double-quantum homonuclear NMR correlation spectroscopy of quadrupolar nuclei subjected to magic-angle spinning and high magnetic field. Journal of magnetic resonance. 2009;200(2) :251-260.

[74] Edén M, Zhou D, Yu J. Improved double-quantum NMR correlation spectroscopy of dipolar-coupled quadrupolar spins. Chemical Physics Letters. 2006;431(4–6):397–403.]

[75] Angeli F, Villain O, Schuller S, Charpentier T, de Ligny D, Bressel L, et al. Effect of temperature and thermal history on borosilicate glass structure. Physical review B. 2012;85(5) :054110.

[76] Massiot D, Fayon F, Capron M, King I, Le Calvé S, Alonso B, et al. Modelling one- and two-dimensional solid-state NMR spectra. Magnetic Resonance in Chemistry. 2002;40(1) :70-76.

[77] Howes A, Vedishcheva N, Samoson A, Hanna JV, Smith ME, Holland D, et al. Boron environments in Pyrex® glass-a high resolution, Double-Rotation NMR and thermodynamic modelling study. Physical Chemistry Chemical Physics. 2011;13(25) :11919-11928.

[78] Clayden N, Esposito S, Aronne A, Pernice P. Solid state ^{11}B NMR study of glasses near the barium metaborate stoichiometry. Journal of non-crystalline solids. 1999;249(2-3) :99-105.

[79] Murakami M, Shimizu T, Tansho M, Akai T, Yazawa T. ^{11}B-^{11}B Two-Dimensional Correlation Nuclear Magnetic Resonance on Sodium Borosilicate Glass. Chemistry letters. 2010;39(1) :32-33.

[80] Wu J, Potuzak M, Stebbins JF. High-temperature in situ ^{11}B NMR study of network dynamics in boron-containing glass-forming liquids. Journal of non-crystalline solids. 2011;357(24) :3944-3951.

[81] Zhang Z, Gustin L, Xie W, Lian J, Valsaraj KT, Wang J. Effect of solution chemistry on the iodine release from iodoapatite in aqueous environments. Journal of Nuclear Materials. 2019;525 :161-170.

[82] Yu Y, Stevensson B, Eden M. Direct experimental evidence for abundant BO_4-BO_4 motifs in borosilicate glasses from double-quantum ^{11}B NMR spectroscopy. The Journal of Physical Chemistry Letters. 2018;9(21) :6372-6376.

[83] Loewenstein W. The distribution of aluminum in the tetrahedra of silicates and aluminates. American Mineralogist: Journal of Earth and Planetary Materials. 1954;39(1-2) :92-96.

[84] Lee SK, Stebbins JF. The degree of aluminum avoidance in aluminosilicate glasses. American Mineralogist. 1999;84(56) :937-945.

[85] Lee SK, Stebbins JF. The structure of aluminosilicate glasses: high-resolution ^{17}O and ^{27}Al MAS and 3QMAS NMR study. The Journal of Physical Chemistry B. 2000;104(17) :4091-4100.

[86] Wright AC. Borate structures: crystalline and vitreous. Physics and Chemistry of Glasses-European Journal of Glass Science and Technology Part B. 2010;51(1) :1-39.

[87] Edén M. Probing oxide-based glass structures by solid-state NMR: Opportunities and limitations. Journal of Magnetic Resonance Open. 2023;16 :100112.

[88] Turner GL, Smith KA, Kirkpatrick RJ, Oldfieldt E. Structure and cation effects on phosphorus-31 NMR chemical shifts and chemical-shift anisotropies of orthophosphates. Journal of Magnetic Resonance (1969). 1986;70(3) :408-415.

[89] Soleilhavoup A, Delaye JM, Angeli F, Caurant D, Charpentier T. Contribution of first-principles calculations to multinuclear NMR analysis of borosilicate glasses. Magnetic Resonance in Chemistry. 2010;48(S1) :S159-S170.

[90] Lo AY, Eden M. Efficient symmetry-based homonuclear dipolar recoupling of quadrupolar spins: double-quantum NMR correlations in amorphous solids. Physical chemistry chemical physics. 2008;10(44) :6635-6644.

[91] Gómez JS, Trébosc J, Duong NT, Pourpoint F, Lafon O, Amoureux JP. Comparison of through-space homonuclear correlations between quadrupolar nuclei in solids. Journal of Magnetic Resonance. 2023;348 :107388.

[92] Lv P, Wang C, Stevensson B, Yu Y, Wang T, Edén M. Impact of the cation field strength on physical properties and structures of alkali and alkaline-earth borosilicate glasses. Ceramics International. 2022;48(13) :18094-18107.

[93] Angeli F, Charpentier T, Gaillard M, Jollivet P. Influence of zirconium on the structure of pristine and leached sodalime borosilicate glasses: Towards a quantitative approach by ^{17}O MQMAS NMR. Journal of non-crystalline solids. 2008;354(31) :3713-3722.

[94] Wu J, Stebbins JF. Effects of cation field strength on the structure of aluminoborosilicate glasses: high-resolution ^{11}B, ^{27}Al and ^{23}Na MAS NMR. Journal of Non-Crystalline Solids. 2009;355(9) :556-562.

[95] Le Caër, G., & Brand, R. A. General models for the distributions of electric field gradients in disordered solids. Journal of Physics: Condensed Matter. 1998;10(47), 10715.

[96] Werner-Zwanziger, U., Paterson, A. L., & Zwanziger, J. W. The Czjzek distribution in solid-state NMR: Scaling properties of central and satellite transitions. Journal of Non-Crystalline Solids. 2020;550, 120383.

[97] Neuville, D. R., Cormier, L., & Massiot, D. Al environment in tectosilicate and peraluminous glasses: A ^{27}Al MQ-MAS NMR, Raman, and XANES investigation. Geochimica et Cosmochimica Acta. 2004;68(24), 5071-5079.

[98] Neuville, D. R., Cormier, L., Montouillout, V., Florian, P., Millot, F., Rifflet, J. C., & Massiot, D. Structure of Mg-and Mg/Ca aluminosilicate glasses: ^{27}Al NMR and Raman spectroscopy investigations. American Mineralogist. 2008;93(11-12), 1721-1731.

[99] Lee, S. K., Deschamps, M., Hiet, J., Massiot, D., & Park, S. Y. Connectivity and proximity between quadrupolar nuclides in oxide glasses: insights from through-bond and through-space correlations in solid-state NMR. The Journal of Physical Chemistry B. 2009;113(15), 5162-5167.

[100] Lo grado, M., Youngman, R. E., Aitken, B. G., & Eckert, H. Network Modifier Effects in Multiple Network Former Glasses: NMR Results on the System 70 SiO_2–7.5 P_2O_5–(22.5–x) Al_2O_3–x Na_2O ($0 \leq x \leq 17.5$). The Journal of Physical Chemistry C. 2023;127(34), 17269-17284.

[101] Wu J, & Stebbins JF. Cation field strength effects on boron coordination in binary borate glasses. Journal of the American Ceramic Society. 2014;97(9), 2794-2801.

[102] Yamashita H, Inoue K, Nakajin T, Inoue H, Maekawa T. Nuclear magnetic resonance studies of 0.139 MO (or M_2O)-0.673SiO_2-(0.188- x)Al_2O_3-xB_2O_3 (M= Mg, Ca, Sr and Ba, M= Na and K) glasses. Journal of non-crystalline solids. 2003;331(1-3) :128-136.

[103] Quintas A, Charpentier T, Majérus O, Caurant D, Dussossoy JL, Vermaut P. NMR study of a rare-earth aluminoborosilicate glass with varying CaO-to-Na_2O ratio. Applied Magnetic Resonance. 2007;32(4) :613-634.

[104] Lu X, Deng L, Du J, Vienna JD. Predicting boron coordination in multicomponent borate and borosilicate glasses using analytical models and machine learning. Journal of Non-Crystalline Solids. 2021 ;553 :120490

[105] Stebbins JF, Wu J, Thompson LM. Interactions between network cation coordination and non-bridging oxygen abundance in oxide glasses and melts: Insights from NMR spectroscopy. Chemical Geology. 2013;346 :34-46.

[106] Morizet Y, Vuilleumier R, Paris M. A NMR and molecular dynamics study of CO_2-bearing basaltic melts and glasses. Chemical Geology. 2015;418 :89-103.

[107] Allwardt JR, Stebbins JF, Terasaki H, Du LS, Frost DJ, Withers AC, et al. Effect of structural transitions on properties of high-pressure silicate melts: ^{27}Al NMR, glass densities, and melt viscosities. American Mineralogist. 2007;92(7) :1093-1104.

[108] Xue, X., & Kanzaki, M. Structure of hydrous aluminosilicate glasses along the diopside–anorthite join: A comprehensive one-and two-dimensional ^{1}H and ^{27}Al NMR study. Geochimica et Cosmochimica Acta. 2008;72(9), 2331-2348.

[109] Le Losq, C., Neuville, D. R., Florian, P., Henderson, G. S., & Massiot, D. The role of Al^{3+} on rheology and structural changes in sodium silicate and aluminosilicate glasses and melts. Geochimica et Cosmochimica Acta. 2014;126, 495-517.

[110] Kelsey KE, Allwardt JR, Stebbins JF. Ca-Mg mixing in aluminosilicate glasses: an investigation using ^{17}O MAS and 3QMAS and ^{27}Al MAS NMR. Journal of Non-Crystalline Solids. 2008;354(40-41) :4644-4653.

[111] Xue X, Stebbins JF, Kanzaki M, McMillan PF, Poe B. Pressure-induced silicon coordination and tetrahedral structural changes in alkali oxide-silica melts up to 12 GPa: NMR, Raman, and infrared spectroscopy. American Mineralogist. 1991;76(1-2) :8-26.

[112] Funamori N, Yamamoto S, Yagi T, Kikegawa T. Exploratory studies of silicate melt structure at high pressures and temperatures by in situ X-ray diffraction. Journal of Geophysical Research: Solid Earth. 2004;109(B3).

[113] Louvel M, Sanchez-Valle C, Malfait WJ, Testemale D, Hazemann JL. Zr complexation in high pressure fluids and silicate melts and implications for the mobilization of HFSE in subduction zones. Geochimica et Cosmochimica Acta. 2013;104 :281-299.

[114] Sanloup C, Drewitt JW, Konôpková Z, Dalladay-Simpson P, Morton DM, Rai N, et al. Structural change in molten basalt at deep mantle conditions. Nature. 2013;503(7474) :104-107.

[115] Lee AC, Lee SK. Network polymerization and cation coordination environments in boron-bearing rhyolitic melts: Insights from ^{17}O, ^{11}B, and ^{27}Al solid-state NMR of sodium aluminoborosilicate glasses with varying boron content. Geochimica et Cosmochimica Acta. 2020;268 :325-347.

931 **FIGURES**

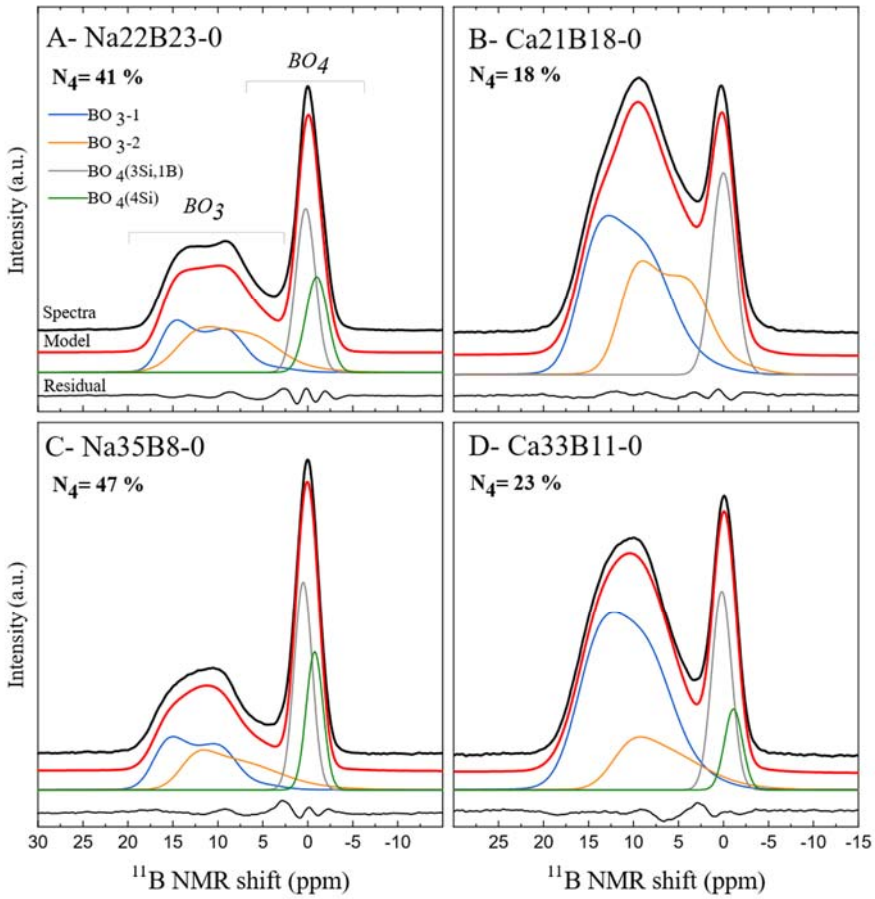

932

933 Figure 1: ^{11}B MAS NMR fitting results for samples recovered from atmospheric pressure
934 experiments. Fits are made with 4 components accounting for BO_3-1, BO_3-2, BO_4(1B,3Si),
935 BO_4(4Si), except for Ca21B18. Result values are presented in Table 2.

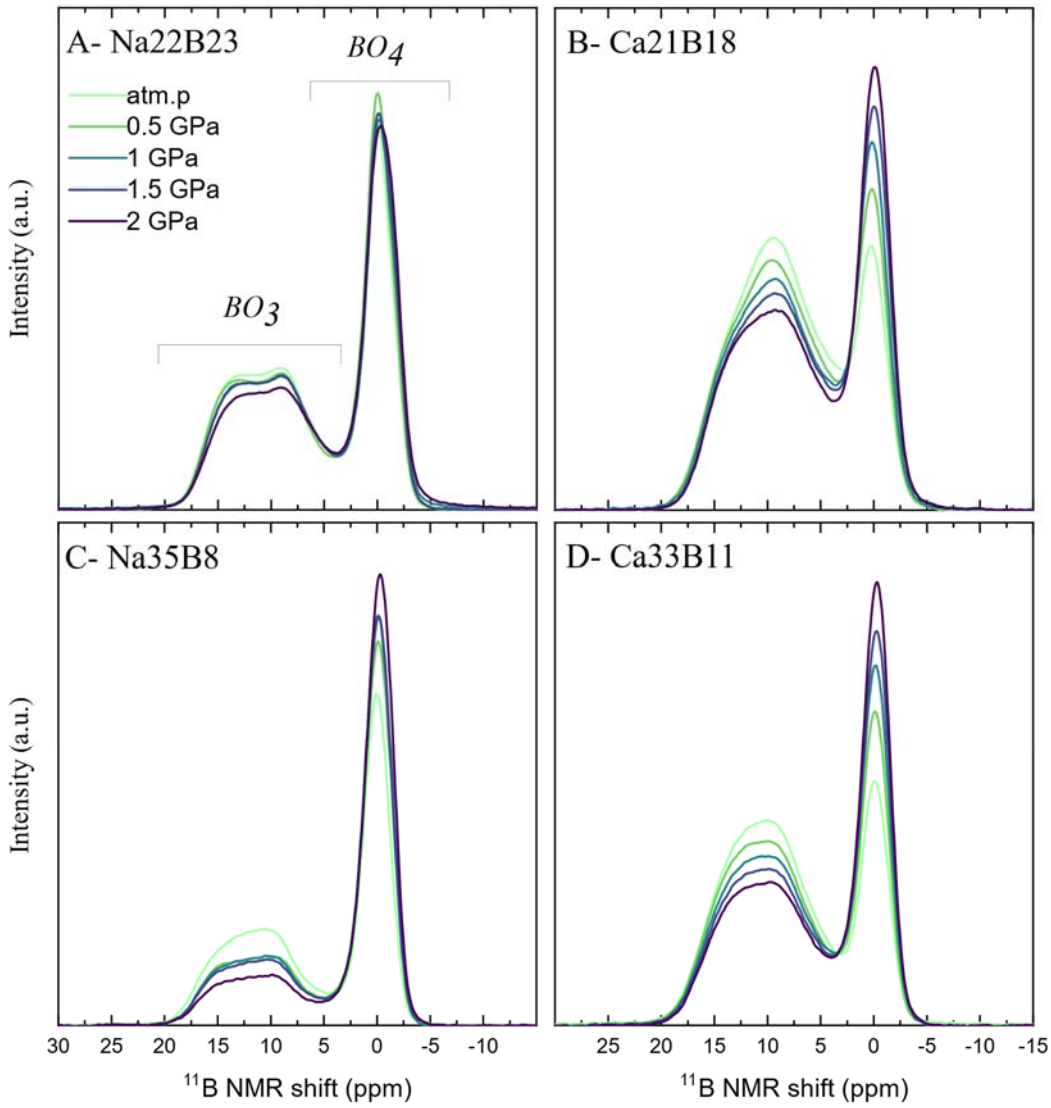

936

937 Figure 2: Superposition of the (area-normalized) ^{11}B MAS NMR spectra. The atmospheric

938 pressure samples have higher BO_3 and lower BO_4 than samples recovered from 2 GPa.

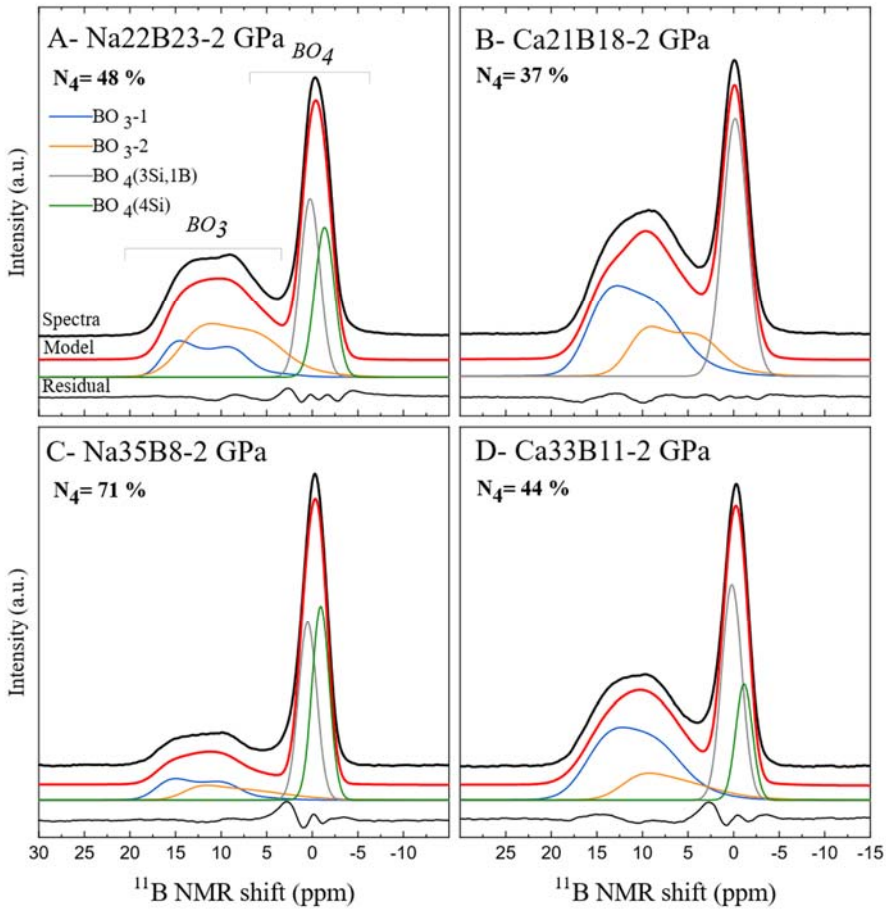

939

940 Figure 3: ^{11}B MAS NMR fitting results for samples recovered from 2 GPa. Fits are made with
941 4 components accounting for BO_3-1, BO_3-2, BO_4(1B,3Si), BO_4(4Si), except for Ca21B18.
942 Result values are presented in Table 2.

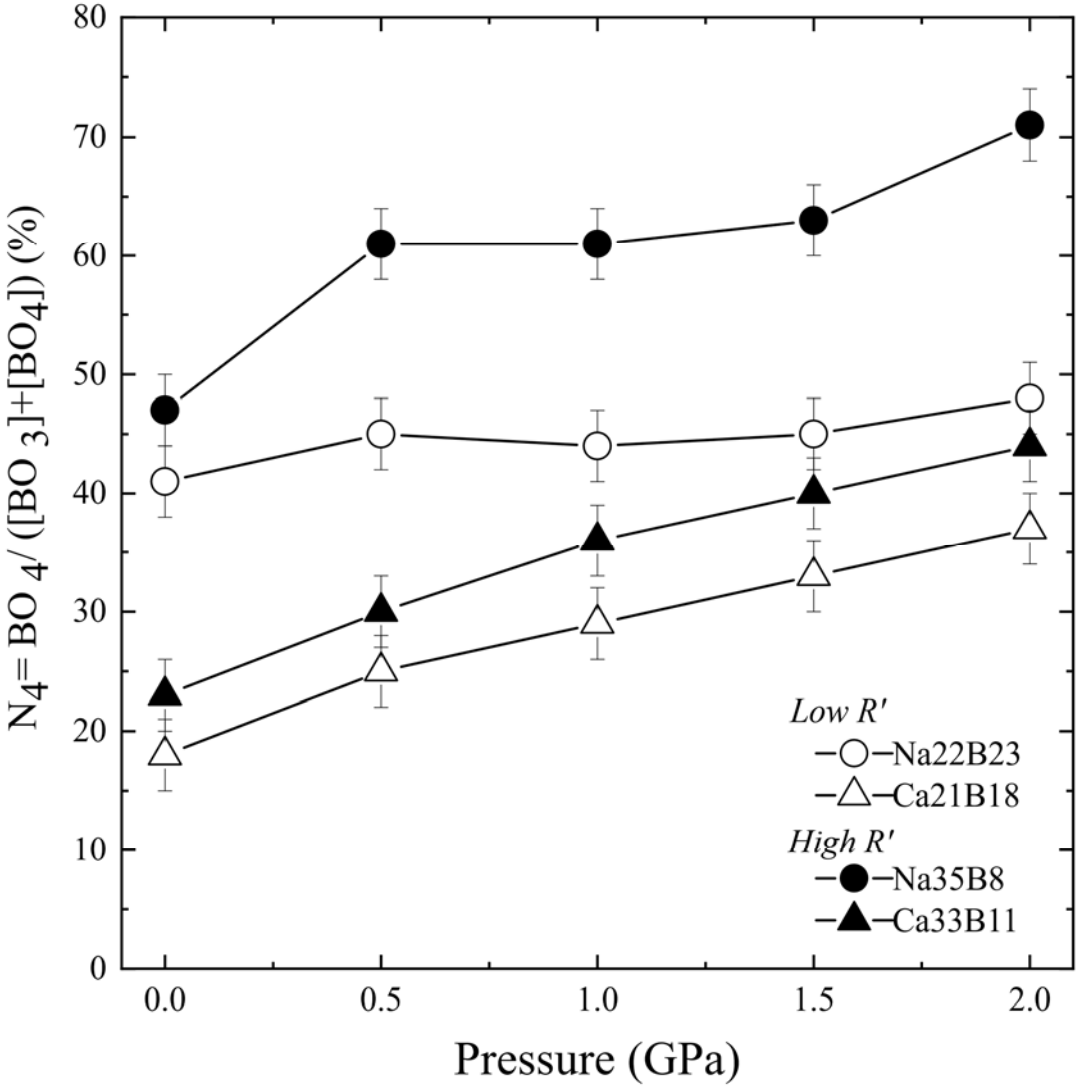

943

944 Figure 4: The fraction of four-coordinated boron (N_4) plotted against the pressure. Open
945 symbols stands for the low-R' samples, full symbols for high-R' samples. Na-bearing samples
946 are plotted with circle and Ca-bearing samples with triangles. Error on N_4 measurement is
947 estimated to ± 3 in %, see Table 2.

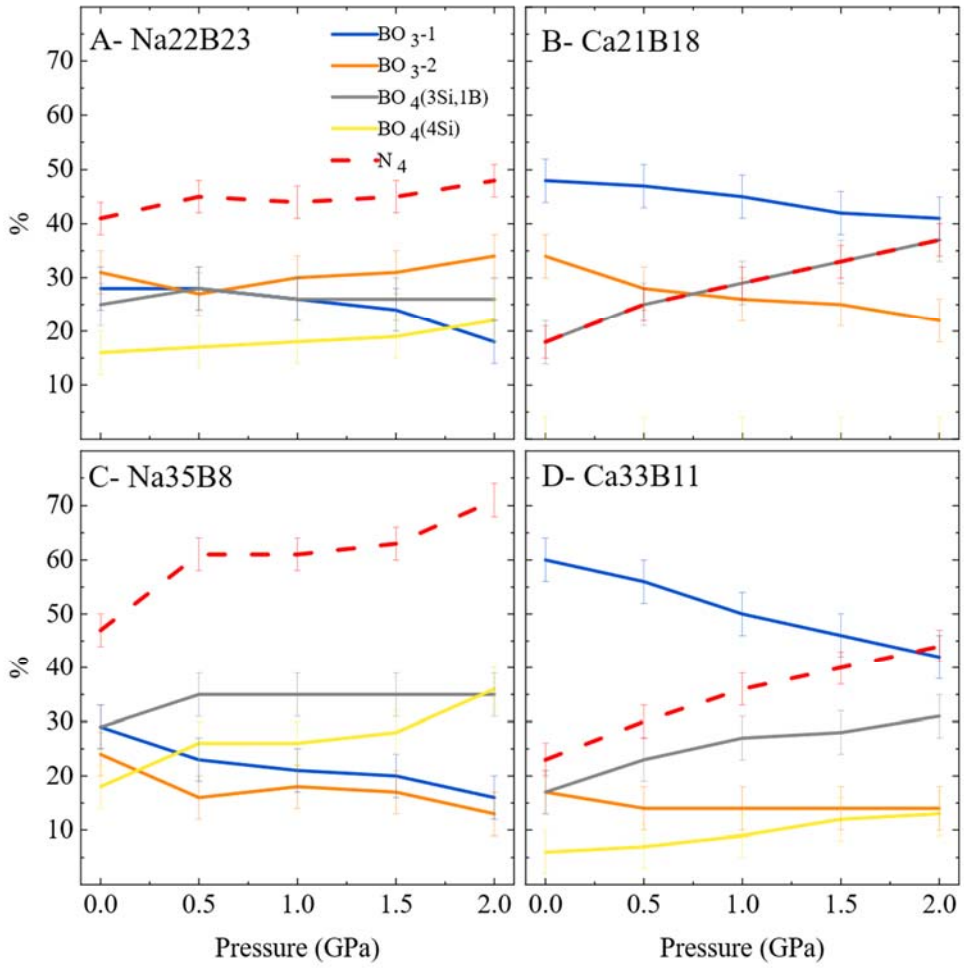

948

949 Figure 5: Results from fits plotted as the proportion of components (BO_3-1, BO_3-2, BO_4(1B,3Si)
950 and BO_4(4Si)) against the pressure. The calculated N_4 is plotted in bold dashed line. Values are
951 presented in Table 2. Error on N_4 measurement and the component proportion is estimated to ±
952 3 in % and to ± 2 in %, respectively, see Table 2.

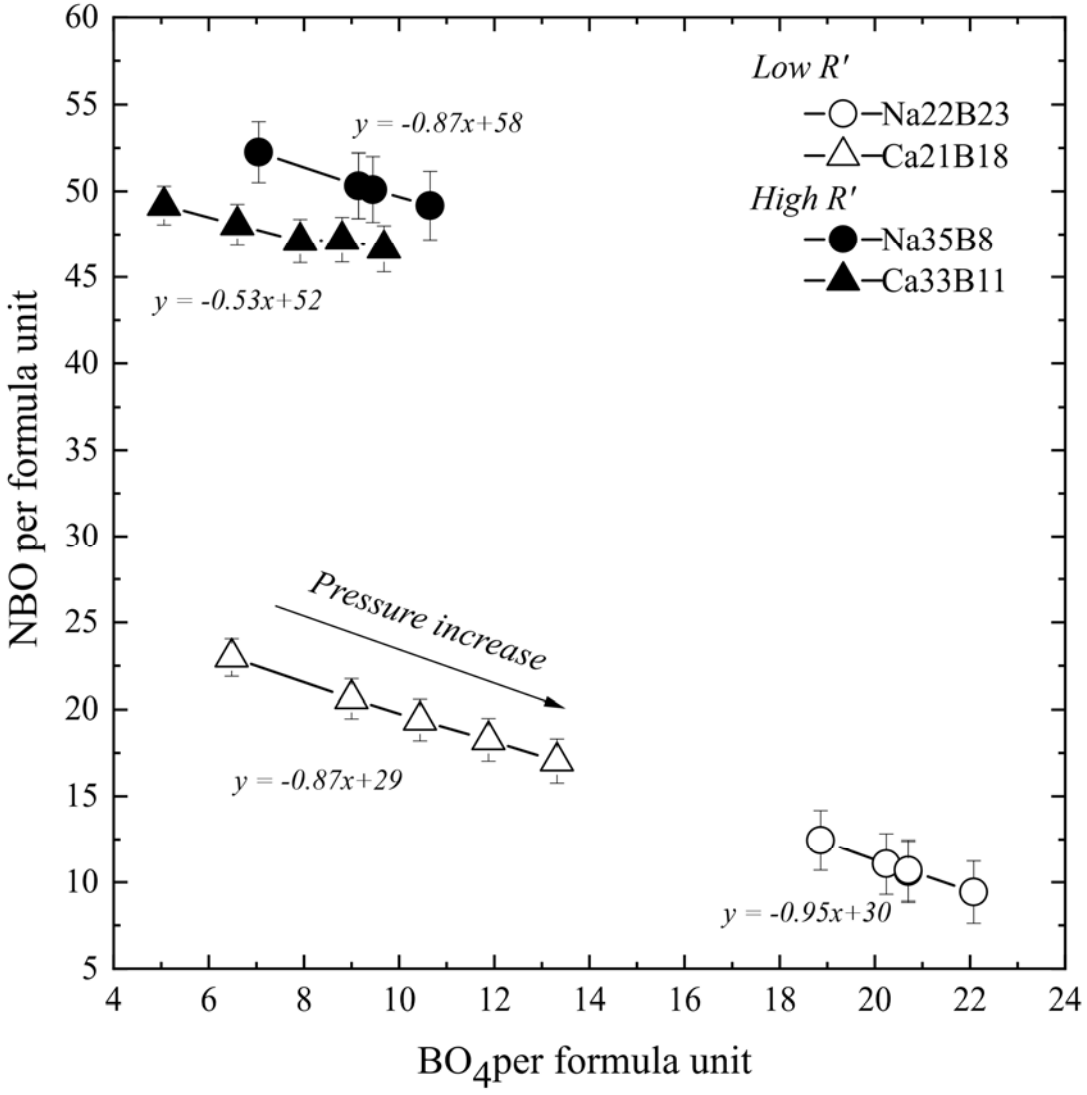

953

954 Figure 6: The calculated proportion of non-bridging oxygen (NBO) plotted against the fraction
955 of four-coordinated boron (N_4). Open symbols stands for the low-R' samples, full symbols for
956 high-R' samples. Na-bearing samples are plotted with circle and Ca-bearing samples with
957 triangles. Error on values have been calculated from errors on N_4, Al_{CN} and composition. Error
958 bars for the BO_4 are within the symbol size.

959

960

961 **TABLES**

962

963 Table 1: Major element compositions and experimental conditions for aluminoborosilicate
964 glasses.

Sample	Major elements in mol.%[a]					R'[b]	K'[b]
	SiO_2	B_2O_3	Al_2O_3	CaO	Na_2O		
Na22B23-0	49.0(2)	23.0(1)	6.2(1)		21.7(3)	0.7	1.7
Ca21B18-0	55.0(4)	18.0(7)	6.3(1)	20.7(2)		0.9	2.3
Na35B8-0	51.4(2)	7.5(9)	5.8(1)		35.3(4)	2.7	3.9
Ca33B11-0	50.1(3)	11.0(5)	6.1(1)	32.8(1)		1.9	2.9

965

966 a The major element concentrations have been determined for the glasses obtained at ambient pressure and are
967 reported in ref. [61]. The SiO_2, Al_2O_3 and Na_2O/CaO have been determined by SEM EDS measurements and the
968 B_2O_3 has been measured using LA ICP MS. The error is reported between brackets and corresponds to the
969 standard deviation derived on several measurements. The details of the analytical conditions can be found in ref.
970 [61].
971 b The R' is determined as follow $[Na_2O]+[CaO]/[B_2O_3]+[Al_2O_3]$; the K' corresponds to the
972 $[SiO_2]/[B_2O_3]+[Al_2O_3]$ ratio.
973

Table 2: ^{11}B MAS NMR fitting results

Sample		Pressure (GPa)	BO_3-1 [a] δ_{iso} (ppm)	FWHM CS (ppm)	Cq (kHz)	FWHM Cq (kHz)	%	BO_3-2 [a] δ_{iso}	FWHM CS	Cq	FWHM Cq	%	BO_4(3Si,1B) [b] δ_{iso}	Width (ppm)	%	BO_4(4Si) [b] δ_{iso}	Width	%	N_4
Na22B23	-0	0.0001	18.2	2.5	2612	250	28	15.9	5.1	2741	350	31			25	-1	2.8	16	41
	-1	0.5					28					27			28	-1.1	2.7	17	45
	-2	1					26					30	0.2	2.6	26	-1.2	2.8	18	44
	-3	1.5					24					31			26	-1.2	2.6	19	45
	-4	2					18					34			26	-1.4	2.5	22	48
Ca21B18	-0	0.0001	17.4	4.1	2600	444	48	13.0	4.0	2623	270	34	0.0	3.1	18	-	-	-	18
	-1	0.5					47					28	0.0	3.1	25	-	-	-	25
	-2	1					45					26	0.0	3.1	29	-	-	-	29
	-3	1.5					42					25	-0.1	3.2	33	-	-	-	33
	-4	2					41					22	-0.2	3.2	37	-	-	-	37
Na35B8	-0	0.0001	18.7	3.0	2550	200	29	15.7	3.5	2750	900	24			29	-0.8	2.2	18	47
	-1	0.5					23					16			35	-1	2.3	26	61
	-2	1					21					18	0.5	2.4	35	-0.9	2.2	26	61
	-3	1.5					20					17			35	-0.9	2.2	28	63
	-4	2					16					13			35	-0.9	2.2	36	71
Ca33B11	-0	0.0001	17.4	5.0	2600	300	60	13.4	4.4	2566	900	17			17	-1.1	2.3	6	23
	-1	0.5					56					14			23	-1.2	2.2	7	30
	-2	1					50					14	0.2	2.6	27	-1.2	2.2	9	36
	-3	1.5					46					14			28	-1.2	2.1	12	40
	-4	2					42					14			31	-1.2	2.2	13	44

a The asymmetry parameter (ηq) were set to 0.2 and 0.0 for BO_3-1 and BO_3-2 lines, respectively. In both cases, no distribution of ηq was considered.

b Quadrupolar coupling constants (Cq) were only determined for the BO_3. The Cq for the tetrahedral BO_4 units are very small, therefore we used Gaussian peak to simulate the line shape.

Estimated uncertainty: ±0.5ppm for δ_{iso} and FWHM CS, ±200 kHz for Cq, ±100 kHz for FWHM Cq (except for FWHM Cq = 900 kHz where the error bar estimated is ±300 kHz), and ±0.3 ppm for the width. While these uncertainties provide a general sense of the data spread based on the adopted fitting protocol, further investigation may be required for a more rigorous error analysis. Errors on each component value is calculated less than ±2 in %, and error on N_4 is calculated less than ±3 in %, both from the Monte Carlo error analysis in the DMfit software [76].

Table 3: Comparison of the measured N_4 with calculation from models, proportions of AlO_4, BO_4 and NBO

Sample		Pressure (GPa)	N_4 model *Du and Stebbins, 2005a*	N_4 model *Lu et al., 2021*	Measured N_4	BO_4 [a] mol.%	Al_{CN} [b]	AlO_4 [a] mol.%	Calculated NBO per formula unit[c]
Na22B23	-0	0.0001	61	45	41	18.9	4.02	12.1	12.4
	-1	0.5			45	20.7	4.02	12.1	10.6
	-2	1			44	20.2	4.02	11.9	11.3
	-3	1.5			45	20.7	4.03	12.0	10.7
	-4	2			48	22.1	4.04	11.9	9.4
Ca21B18	-0	0.0001	64	24	18	6.5	4.06	11.9	23.0
	-1	0.5			25	9	4.08	11.8	20.6
	-2	1			29	10.4	4.10	11.6	19.4
	-3	1.5			33	11.9	4.14	11.3	18.3
	-4	2			37	13.3	4.16	11.0	17.0
Na35B8	-0	0.0001	54	59	47	7.1	4.03	11.3	52.3
	-1	0.5			61	9.2	4.04	11.1	50.3
	-2	1			61	9.2	4.04	11.1	50.3
	-3	1.5			63	9.5	4.05	11.1	50.1
	-4	2			71	10.7	4.08	10.8	49.2
Ca33B11	-0	0.0001	56	46	23	5.1	4.08	11.4	49.2
	-1	0.5			30	6.6	4.11	11.0	48.0
	-2	1			36	7.9	4.15	10.6	47.1
	-3	1.5			40	8.8	4.25	9.6	47.2
	-4	2			44	9.7	4.29	9.3	46.7

a AlO_4 % = $^4Al.2.[Al_2O_3]$ with associated error better than ±0.6; BO_4 % = $N_4.2.[B_2O_3]$ with associated error better than ±0.8.

b Average aluminium coordination number $Al_{CN} = 4.[^4Al]+5.[^5Al]+6.[^6Al]$ with associated error better than ±0.05.

c Calculated NBO content per formula unit: $NBO = 2.[Na_2O+CaO]-[AlO_4+BO_4]$ with associated error better than ±2 in %.